Colloids and Surfaces B: Biointerfaces 128 (2015) 106–114

Contents lists available at ScienceDirect

Colloids and Surfaces B: Biointerfaces

journal homepage: www.elsevier.com/locate/colsurfb

Electrospun poly(L-lactic acid-co-ε-caprolactone) fibers loaded with heparin and vascular endothelial growth factor to improve blood compatibility and endothelial progenitor cell proliferation

Xi Chen[a,1], Jing Wang[b,1], Qingzhu An[a], Dawei Li[b], Peixi Liu[a], Wei Zhu[a,*], Xiumei Mo[b,*]

[a] Department of Neurosurgery, Huashan Hospital of Fudan University, Shanghai 200040, China
[b] Biomaterials and Tissue Engineering Laboratory, College of Chemistry & Chemical Engineering and Biotechnology, Donghua University, Shanghai 201620, China

ARTICLE INFO

Article history:
Received 9 October 2014
Received in revised form 18 January 2015
Accepted 11 February 2015
Available online 19 February 2015

Keywords:
Electrospun fibers
Heparin
Vascular endothelial growth factor
Blood compatibility
Endothelial progenitor cell

ABSTRACT

Emulsion electrospinning is a convenient and promising method for incorporating proteins and drugs into nanofiber scaffolds. The aim of this study was to fabricate a nanofiber scaffold for anticoagulation and rapid endothelialization. For this purpose, we encapsulated heparin and vascular endothelial growth factor (VEGF) into the core of poly(L-lactic acid-co-ε-caprolactone) (P(LLA-CL)) core–shell nanofibers via emulsion electrospinning. The fiber morphology, core–shell structure and hydrophilicity of the nanofiber mats were analyzed by scanning electron microscopy, transmission electron microscopy and water contact angle. The blood compatibility was measured by hemolysis and anticoagulation testing. A CCK-8 assay was performed to study the promotion of endothelial progenitor cell (EPC) growth and was complemented by immunofluorescent staining and SEM. Our study demonstrates that heparin and VEGF can be incorporated into P(LLA-CL) nanofibers via emulsion. The released heparin performed well as an anticoagulant, and the released VEGF promoted EPC growth on the fiber scaffolds. These results imply that electrospun P(LLA-CL) nanofibers containing heparin and VEGF have great potential in the development of vascular grafts in cases where antithrombogenicity and accelerated endothelialization are desirable.

1. Introduction

Vascular grafts have been widely used for decades in the treatment of vascular diseases, such as cardiovascular or peripheral vascular occlusion, renal failure and abdominal arterial aneurysms. Autologous vessels are commonly recommended for this procedure, but in some cases, insufficient or ineligible donor vessels necessitate the use of alternative synthetic grafts. Vascular prostheses made from synthetic polymers, such as expanded polytetrafluoroethylene (ePTFE) and polyethylene terephthalate (PET), have performed favorably in large arteries, but small-caliber grafts (especially those with diameters less than 6 mm) continue to have a high failure rate [1]. Acute thrombogenesis and intimal hyperplasia are believed to be the major causes of failure [2]. The endothelium, a monolayer between the circulating blood and the vascular wall, is a non-thrombogenic interface that plays an important role in the prevention of intimal hyperplasia. Vascular grafts must not only discourage platelet aggregation but also promote rapid endothelialization on the graft surface. For this purpose, researchers have tried modifying graft surfaces with bioactive molecules. Heparin, an anticoagulant with a long history of clinical application [3], has often been incorporated into biomaterials to inhibit thrombogenesis [4–6]. Vascular endothelial growth factor (VEGF) is another potentially effective molecule, as it is involved in two manners of endothelialization [7,8]. Endothelialization used to be attributed solely to the migration and proliferation of the surrounding mature endothelial cells (ECs). It has been demonstrated, however, that peripheral blood contains a unique subgroup of circulating cells with markers similar to those of embryonal angioblasts that have the potential to differentiate into mature ECs [9,10]. These bone marrow-derived cells are called endothelial progenitor cells (EPCs). Mature ECs are terminally programmed cells with low proliferative potential and, as a result, a limited capacity to form a new endothelium layer. EPCs, by contrast, are highly productive and readily available from a self-renewing source, peripheral blood. Thus, they are better for use in vascular therapy.

Although the benefits of VEGF for EPC proliferation have been demonstrated [7], VEGF has a very short half-life in vivo [11], so it is crucial for the delivery vehicle to protect its bioactivity and

* Corresponding authors. Tel.: +86 021 52889999; fax: +86 021 52889999.
E-mail addresses: drzhuwei@fudan.edu.cn (W. Zhu), xmm@dhu.edu.cn (X. Mo).
[1] These authors contributed equally to this work.

http://dx.doi.org/10.1016/j.colsurfb.2015.02.023
0927-7765/

release it at a relatively slow, controlled rate. Electrospinning is a convenient and promising method for fabricating fibers with diameters ranging from several micrometers down to less than 100 nm. The ultrafine diameter of electrospun fibers enables a high specific surface area and porosity. Additionally, electrospun biodegradable nanofibrous polymer scaffolds have a physical structure similar to that of the natural extracellular matrix [12]. Their between-fiber bonding structure promotes cell adhesion, migration and distribution throughout the entire fibrous mat, making biocompatible and biodegradable electrospun nanofibrous mats interesting as tissue engineering scaffolds for biomedical applications. Core–shell structured electrospun nanofibers prepared by coaxial or emulsion electrospinning have potential for use as drug delivery systems because they can encapsulate several types of proteins and drugs [13,14]. The fibers can temporarily protect unstable biological agents and slow the delivery of bioactive molecules or drugs, avoiding a sudden initial burst in their delivery. Emulsion electrospinning is similar to normal solution electrospinning except that the solution is replaced by an emulsion. The droplets dispersed in the emulsion become the core of the fiber, and the continuous matrix becomes the shell [15]. Emulsion electrospinning is a novel approach to the fabrication of core–shell nanofibers for encapsulating proteins and drugs [16]. The most promising application of emulsion electrospinning is the delivery of hydrophilic drugs or bioactive molecules via W/O emulsion to avoid burst release and prolong the release time. Great efforts have been made to incorporate model drugs into electrospun nanofibers for drug delivery via emulsion electrospinning. Chew et al. encapsulated human β-nerve growth factor (NGF) stabilized with BSA into a copolymer of ε-caprolactone and ethyl ethylene phosphate via emulsion electrospinning, thereby allowing the NGF to be released from the fibers in a sustained manner for at least 3 months [17].

Based on our group's preliminary research, we encapsulated different amounts of heparin into a poly(L-lactic acid-co-ε-caprolactone) (P(LLA-CL)) nanofiber mat via emulsion electrospinning and tested the blood compatibility. We then selected the optimal heparin concentration and encapsulated it along with VEGF into the nanofiber mat. P(LLA-CL) (50:50) is a synthetic co-polymer of lactic acid and caprolactone. It is nontoxic, biodegradable, and highly viscoelastic and has been investigated as a biomaterial for use in surgery and drug delivery systems [18]. A previous study showed that it supported the attachment of animal cells and promoted proliferation [19]. We investigated the influence of encapsulated VEGF on EPCs using a CCK assay. Our studies showed that the VEGF released from nanofibers promoted the proliferation of EPCs cultured on the fiber mat surface, demonstrating its potential as a delivery vehicle for the treatment of vascular disease.

2. Materials and methods

2.1. Materials

P(LLA-CL) (LA:CL = 50:50, Mw 300 kDa) was purchased from Gunze Limited, Japan. Heparin (Hep, ≥150 U/mg), sorbitan monooleate (Span 80), dichloromethane and hexafluoroisopropanol (HFIP) were purchased from Shanghai Fine Chemicals (China). Recombinant human VEGF165 was supplied by Peprotech (USA). VEGF ELISA Kit and CCK-8 were purchased from Neobioscience Technology Company (China) and Beyotime Biotech (China), respectively. Lymphocyte separating medium was purchased from MP Biomedics (USA). EGM-2 medium was purchased from Lonza (Switzerland). Ac-LDL and UEA-1-lectin were purchased from Molecular Probe (USA) and Sigma–Aldrich (USA), respectively. The primary antibodies raised against rat CD34 and VEGFR-2 were purchased from R&D systems (USA) and Abcam (UK), respectively. The secondary antibodies were purchased from Molecular Probes (USA). All of the materials and reagents were used without further purification.

2.2. Preparation of electrospinning solution

Emulsions for heparin-containing nanofiber mats were prepared by dissolving different amounts of heparin in distilled water to produce aqueous solutions of 5 wt%, 10 wt% and 15 wt% heparin. Next, for each concentration, 0.25 mL of the aqueous solution and 0.05 mL of Span 80 were added dropwise into 5 mL of methylene dichloride and stirred magnetically to form a uniform water-in-oil emulsion. Next, 0.4 g of P(LLA-CL) was dissolved in the emulsion, and the mixture was stirred overnight to obtain a uniform electrospinning solution. For convenience, the nanofiber scaffolds fabricated with different heparin concentrations via the aforementioned electrospinning solution are abbreviated here as PLCL-5Hep, PLCL-10Hep and PLCL-15Hep, respectively.

After evaluating the blood compatibility of the heparin-containing scaffolds, we determined the optimal heparin concentration and used that for the rest of the study. After determining the optimal heparin load, a similar process was used for VEGF encapsulated in nanofibers. Heparin and VEGF emulsions were prepared by adding different volumes of aqueous VEGF into aqueous heparin solutions at the optimized concentration, thereby obtaining mixed solutions with 0 μg, 10 μg, 20 μg and 30 μg of VEGF and heparin per mL. Next, 0.5 mL of this mixed solution and 0.05 mL of Span 80 were added into 5 mL of dichloromethane and stirred to create a uniform emulsion. As before, 0.4 g of P(LLA-CL) was then dissolved into the emulsions, and the mixtures were stirred overnight to obtain a uniform electrospinning solution. For convenience, the nanofiber scaffolds fabricated from these solutions are abbreviated here as PLCL-Hep, PLCL-Hep-10VEGF, PLCL-Hep-20VEGF and PLCL-Hep-30VEGF. Details of the solutions used to fabricate these four different nanofiber mats are shown in Supplementary Table 1.

Supplementary material related to this article can be found, in the online version, at http://dx.doi.org/10.1016/j.colsurfb.2015.02.023.

A nanofiber scaffold fabricated from an emulsion containing no heparin or VEGF, only deionized water, served as the control (named PLCL-W). Pure P(LLA-CL) electrospinning solution was prepared by dissolving 0.4 g of P(LLA-CL) in 5 mL of HFIP, and the obtained nanofiber mat, named PLCL, also served as a control scaffold.

2.3. Electrospinning the nanofibers

The experimental electrospinning set-up included a voltage power supply (BGG DC high-voltage generator) purchased from BMEI Co., Ltd. (Beijing, China) and a digitally controlled, highly accurate syringe pump (KDS 200) purchased from KD Scientific (Holliston, Massachusetts). The polymer solutions were fed separately into a 5-mL standard syringe attached to a 9 G blunted stainless steel needle. During electrospinning, 14 kV was applied at the tip of the syringe needle. The electrospinning solution flow rate was maintained at 1.0 mL/h. The electrospun fibers were collected on an electrically grounded piece of aluminum foil approximately 12 cm below the tip of the needle. The electrospinning was conducted under ambient conditions. The collected nanofibers were dried overnight under vacuum to remove residual organic solvent. Prior to biological testing, all of the nanofibrous mats were rinsed 3 times with normal saline to remove superficial impurities and were stored at 4 °C after drying.

The nanofiber mats used to evaluate cell compatibility were fabricated by the following method. Medical-grade cover-slips (14 mm in diameter) were placed on the aluminum foil to collect the

nanofiber mats during electrospinning. Once the slips were covered with 50-μm-thick nanofiber mats, they were removed from the aluminum foil and fixed on 24-well plates by stainless steel rings. The scaffolds were further sterilized with 75 vol% ethanol. After sterilization, the samples were washed three times with phosphate-buffered saline solution (PBS).

2.4. Characterization of electrospun nanofibers

2.4.1. Nanofiber morphology and structure

The surface morphology of the fabricated nanofibers was examined using a JSm-5600 LV digital vacuum Scanning Electron Microscope (SEM) produced by the Japan Electron Optical Laboratory (JEOL). SEM samples were sputter-coated with gold prior to examination. The nanofiber diameters were calculated with ImageJ 1.3 (National Institutes of Health, USA) image visualization software. Average fiber diameters and diameter distributions were determined by measuring approximately 100 random fibers in the SEM micrographs. The composite nanofibers' interior structure was analyzed using transmission electron microscopy (TEM) (H-800, Hitachi) at 100 KeV. The TEM samples were prepared by directly depositing emulsion electrospun nanofibers onto carbon-coated copper grids. To study the distribution of VEGF in the nanofibers, fluorescein isothiocyanate conjugated BSA (FITC-BSA) was used as the stabilizer, and the FITC-BSA distribution in the fabricated nanofibers was observed by laser scanning confocal microscopy (LSCM) (Zeiss LSM 700, Germany).

2.4.2. Water contact angles of nanofiber

Water contact angles were measured using a contact angle analyzer (Data Physics Corp., San Jose, CA, USA) to determine the hydrophilicity/hydrophobicity of the nanofiber mats. To measure the contact angles, the mats were cut into 1-cm^2 squares and placed on a testing plate. Next, 0.03 mL of deionized water was dropped onto the specimens. The contact angle between the water droplet and the nanofiber mat was measured at various time intervals at three different locations on the sample. The average value and standard deviation ($\pm$SD) were recorded for each sample.

2.4.3. In vitro release profile of heparin and VEGF

The controlled release of heparin and VEGF from the fiber mats was studied. The fiber mats of PLCL-15Hep-10VEGF and PLCL-15Hep-20VEGF, each weighing approximately 50 mg (encapsulating approximately 4.5 mg of heparin and 1.25 or 2.5 μg of VEGF, respectively) were soaked in 5 mL of PBS solution in a centrifuge tube. The fiber mats were incubated at 37 °C in a shaker. At various time points, 1 mL of the supernatant was removed from the centrifuge tube and replaced by an equal volume of fresh medium. The actual amounts of heparin and VEGF released from the fiber mats were detected using toluidine blue and an enzyme-linked immunosorbent assay kit (VEGF ELISA), respectively.

2.4.4. In vitro hemocompatibility and biocompatibility tests

2.4.4.1. Collection and handling of human blood. Blood samples were collected from healthy human volunteers (an informed consent statement was signed by every volunteer before any tests were performed) who had a normal blood index determined by routine examination and passed a coagulation function test. The first 3 mL of blood was discarded to prevent contamination by tissue thromboplastin caused by needle puncture. For the platelet adhesion and hemolysis tests, freshly drawn blood samples were injected into containers (BD Blood Collection Vacutainer) containing 3.5 mg of K2 EDTA for anticoagulation. For the platelet adhesion test, anticoagulated human blood was centrifuged at a rate of 1000 rpm for 10 min to obtain platelet-rich plasma. For the hemolysis test, normal saline was used to dilute the blood at a 4:5 ratio by volume.

2.5. Hemolysis test

The hemolysis test was conducted following procedures described in a previous study [20]. Each of the four fiber types was dipped into 15-mL centrifuge tubes containing 10 mL of normal saline previously incubated in a water bath at 37 °C for 30 min. Next, 0.2 mL of the aforementioned diluted blood was added to the tubes, and the mixture was incubated at 37 °C for 60 min. Ten milliliters of normal saline solution/double distilled water combined with 0.2 mL of diluted blood was used as negative/positive controls. After incubation, the fibers were removed, and all of the tubes were centrifuged at 3000 rpm for 10 min. One hundred microliters of the supernatant from each tube were transferred into the wells of a 96-well plate, and the absorbance was measured with a microplate reader (BioTek, USA) at 545 nm. The absorbance of the supernatants from the nanofiber mats and the positive and negative controls were recorded as A_{bs}, A_{bpc} and A_{bnc}, respectively. The hemolysis rates were calculated using the following formula:

$$\text{Hemolysis rate} = \frac{A_{bs} - A_{bnc}}{A_{bpc} - A_{bnc}} \times 100\%.$$

The experiments were run in triplicate and repeated twice.

2.6. Platelet adhesion test

Heparin-containing nanofiber and pure PLCL nanofiber mats were placed in a 24-well plate, and 0.5 mL of platelet-rich plasma was overlaid onto each sample and incubated at 37 °C. After 1 h, the samples were gently rinsed with normal saline to remove any nonspecifically adhered platelets, then fixed with glutaraldehyde, dehydrated in a graded ethanol series and freeze-dried. Finally, all of the nanofiber mats were sputter-coated with gold for SEM observation. For each type, the number of platelets was counted at 3 random locations to calculate the adhesion.

2.7. EPC culture and identification

Animal procedures followed a protocol approved by the Institutional Animal Care and Use Committee (IACUC), and the experimental protocol was approved by the Ethics Committee of Fudan University, Shanghai, China. Bone marrow cells were obtained by flushing the tibias and femurs of Sprague-Dawley rats (Animal Experiment Center, Fudan University) weighing approximately 200–250 g. Low-density bone marrow mononuclear cells were isolated by density gradient centrifugation with lymphocyte separating medium according to the manufacturer's instructions. Freshly isolated low-density mononuclear cells were resuspended in culture medium (EGM-2) consisting of endothelial basal medium, 5% fetal bovine serum, hEGF, VEGF, hFGF-B, IGF-1, ascorbic acid and heparin before they were counted manually. Finally, 1×10^7 mononuclear cells per well were seeded on fibronectin-coated 6-well plates and incubated in a 5% CO_2 incubator at 37 °C. Under daily observation, the medium was first changed 4 days after plating. The medium was changed every 3 days thereafter. The endothelial characteristics of the attached spindle-shaped cells were examined after Ac-LDL uptake and chemical binding with FITC-conjugated UEA-1-lectin. The presence of EPCs was confirmed by imaging double-positive cells via fluorescence microscopy. To further determine that the attached cells had the characteristics of EPCs, fluorescence-activated cell sorting (FACS) was performed to detect CD34 and VEGFR-2(KDR).

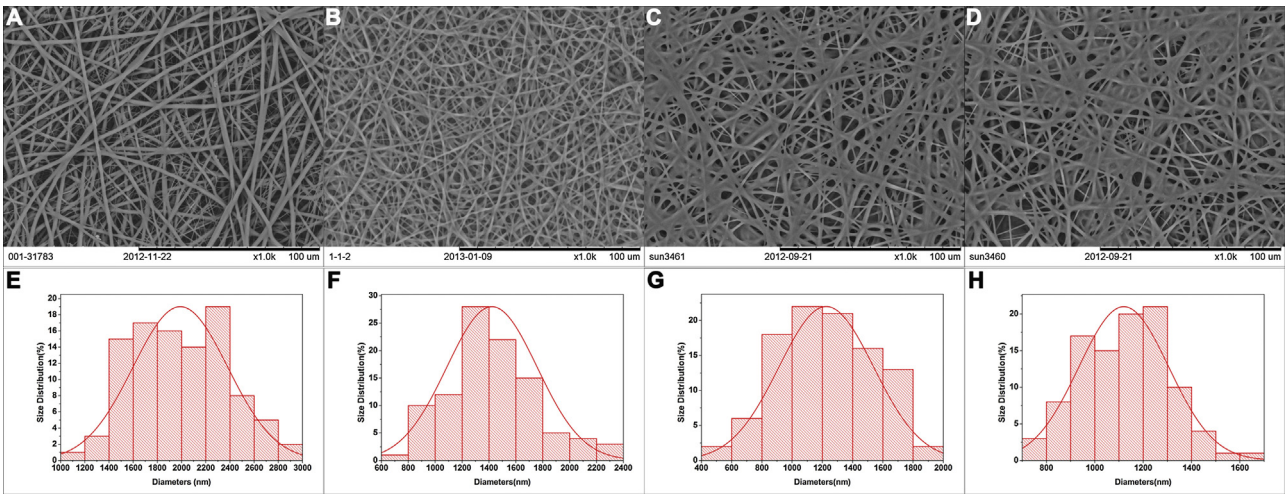

Fig. 1. SEM images of electrospun nanofibers of (A) pure PLCL, (B) PLCL-W, (C) PLCL-Hep, and (D) PLCL-Hep-20VEGF. The fiber diameter distributions of (E) PLCL, (F) PLCL-W, (G) PLCL-Hep, and (H) PLCL-Hep-20VEGF.

2.8. Cell viability test

Cell viability was measured using a cell counting kit-8 (CCK-8) assay. CCK-8 is a sensitive colorimetric assay based on WST-8 and is used to determine the number of viable cells in a cell proliferation or cytotoxicity test. An advantage of the CCK-8 assay over the MTT assay is that WST-8 can be reduced by dehydrogenase in mitochondria to an orange, water-soluble compound, formazan, with low cell toxicity. The amount of formazan is directly proportional to the number of living cells, and the more viable cells there are, the darker the orange solution will become. In this study, P3 EPCs were seeded in three 24-well plates (Fig. 8a) at a cell density of 2×10^4 cells per well and grown at 37 °C for 1, 4 and 7 days. During this procedure, 1 mL of medium was added to each well, and the medium was not changed until the CCK-8 assay test. Next, following the manufacturer's instructions, CCK-8 solution was added to the cell culture medium up to a final concentration of 10 μL/100 μL, and the samples were incubated for another 2 h at 37 °C. Next, 100 μL of solution from each well was transferred into the wells of a 96-well plate, where the absorbance was measured with a microplate reader (BioTek, USA) at 490 nm to determine the cell viability. In addition, another two plates were cultured under the same conditions for 7 days, one for immunofluorescent staining, the other for SEM. Immunofluorescent staining with DAPI and Rhodamine was performed to show the morphology and quantity of EPCs; SEM was performed to directly observe EPCs on the surface of different nanofiber mats.

2.9. Statistical analysis

The results are expressed as the means ± standard deviations. Statistical analysis was performed using Origin 8.0 (OriginLab, Northampton, MA). Significant differences were determined using one-way ANOVA; the data were considered statistically significant at $p < 0.05$.

3. Results and discussion

When performing emulsion electrospinning, selecting an emulsifier capable of creating a homogeneous and stable emulsion is crucial. Span 80 was chosen as the emulsifier in this study for its nontoxicity and good emulsifying ability. After adding Span 80, it was found that the aqueous solutions were well dispersed throughout the organic solutions upon stirring; the emulsions remained homogeneous and stable for several days.

3.1. Nanofiber morphology and structure

Many parameters affect fiber morphology and diameter during electrospinning. The composition of the emulsion has a significant effect on the fiber morphology. If the emulsion droplets are significantly elongated, parts of them can break off into smaller droplets due to the electric forces [21]. The emulsion jet produces ultrafine fibers with incorporated proteins and/or drugs when the solvent evaporates. SEM micrographs of the four different types of electrospun nanofiber scaffolds are shown in Fig. 1. It can be observed that the nanofibers are uniform, with smooth surfaces and a beadless nano-scaled fibrous structure. The fiber diameters of the PLCL, PLCL-W, PLCL-Hep, and PLCL-Hep-20VEGF nanofiber scaffolds were in the ranges of 1989 ± 392, 1422 ± 336, 1225 ± 313, 1119 ± 186 nm, respectively (Fig. 1). This finding reveals that heparin/VEGF-embedded nanofibers had smaller diameters than pure PLCL nanofibers produced by the same electrospinning process. Because the Span 80 molecule has a highly hydrophilic end that can interact with the heparin and VEGF molecules, Span 80/heparin and/or VEGF complexes carry more charge during the process of electrospinning [22]. Furthermore, it is well known that the polymer jets with higher conductivity can be elongated more easily and generate much thinner nanofibers.

Moreover, it is clear that the fibers (PLCL-W, PLCL-Hep, PLCL-Hep-20 VEGF) conglutinated at their junction zone because water in the emulsion, with its relatively low volatility, was not able to completely evaporate when the surfactant was added.

The interior structure of the composite fibers was investigated with TEM. The TEM micrographs revealed that the PLCL-W nanofibers had a continuous core–shell structure (Fig. 2A–C), while the nanofibers incorporating heparin and/or VEGF had a discontinuous multicore–shell structure. Heparin and VEGF were observed to have a zonal distribution inside the nanofibers (Fig. 2B and C). This phenomenon may indicate that the strong negative charge induced by the heparin increased the inter-droplet repulsive force, making it difficult to form a continuous core–shell structure during stretching and evaporation. BSA is usually used as the carrier protein to protect the bioactivity of growth factors. So the FITC-BSA was used to confirm the distribution of VEGF in the core of nanofibers. Fig. 2D is the fluorescent image of the nanofibers containing heparin, VEGF and FITC-BSA. The result observed by LSCM

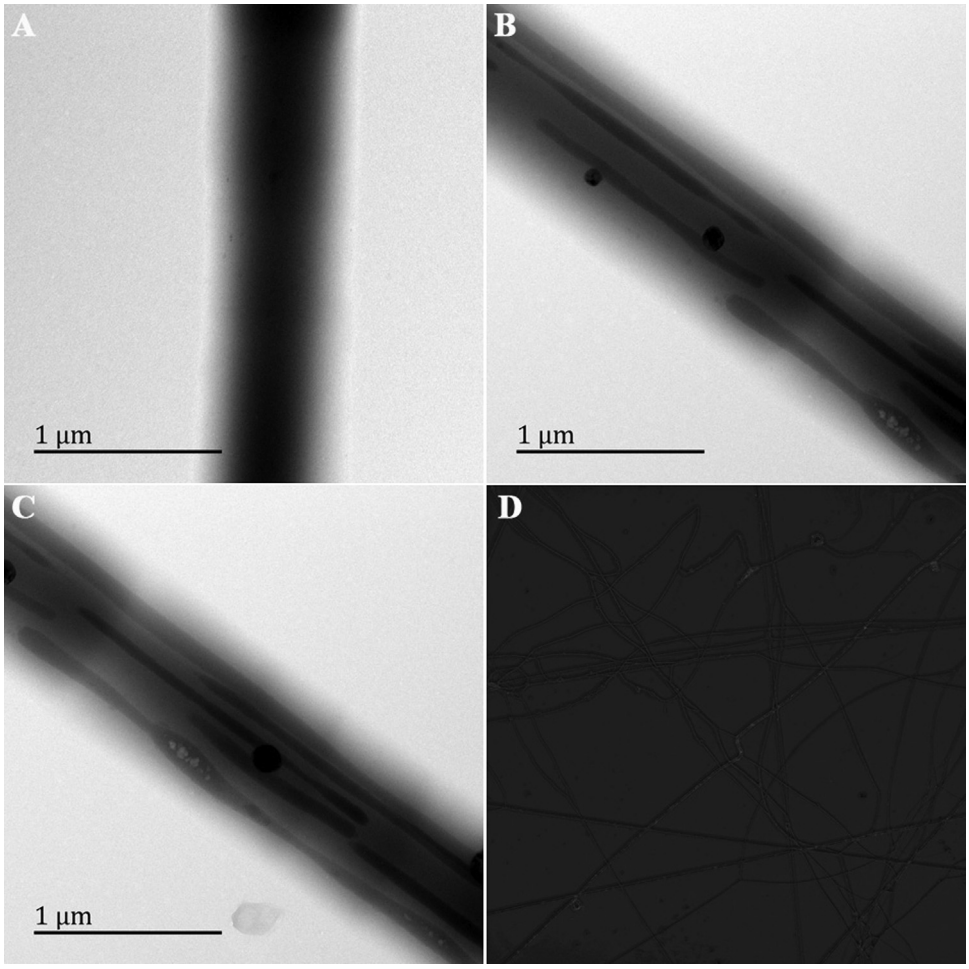

Fig. 2. TEM images of emulsion electrospun nanofibers of (A) PLCL-W, (B) PLCL-Hep, (C) PLCL-Hep-20VEGF and (D) confocal image of fibers of PLCL-Hep-20VEGF with FITC-BSA.

indicated the distribution of FITC-BSA inside the nanofibers. The emitted green fluorescent light suggested the presence of proteins in the nanofibers.

3.2. Water contact angles of the nanofibers

Hydrophilicity is an important factor in the overall performance of electrospun nanofiber mats as tissue engineering scaffolds for cell growth. Adhesion is one of the most important steps after the scaffolds are seeded with cells, followed by cell proliferation and differentiation. Proper hydrophilicity is conducive to adhesion of the cells to the scaffold [23], and according to H Y Wang's study [24], a hydrophilic surface with the water contact angle ranging from 55° to 75° is appropriate for human umbilical vein endothelial cells (HUVECs) to grow on. In this study, the hydrophilicity of the electrospun nanofiber mat was characterized by water contact angle measurements. Fig. 3 shows the contact angle measurement results for stable water droplets placed on the nanofiber mats. The final contact angles of PLCL, PLCL-W, PLCL-Hep and PLCL-Hep-20VEGF scaffolds were $123.71 \pm 3.62°$, $61.80 \pm 2.19°$, $58.08 \pm 3.36°$, $51.73 \pm 3.58°$, respectively. The addition of Span 80, heparin and VEGF reduced the contact angle. PLCL-W nanofiber mats containing emulsifier were much more hydrophilic than pure PLCL nanofiber mats. Additionally, the incorporation of heparin and VEGF slightly improved the hydrophilicity of the nanofiber mats (PLCL-Hep and PLCL-Hep-20 VEGF) because of the larger number of hydrophilic proteins on or near the fiber surface. Thus, this suggests that the incorporation of heparin and VEGF could make these mats even more conducive to cell adhesion and proliferation.

3.3. In vitro release profile of heparin and VEGF

The amounts of heparin and VEGF per milliliter released into the media at different time points are shown in Fig. 4. The release

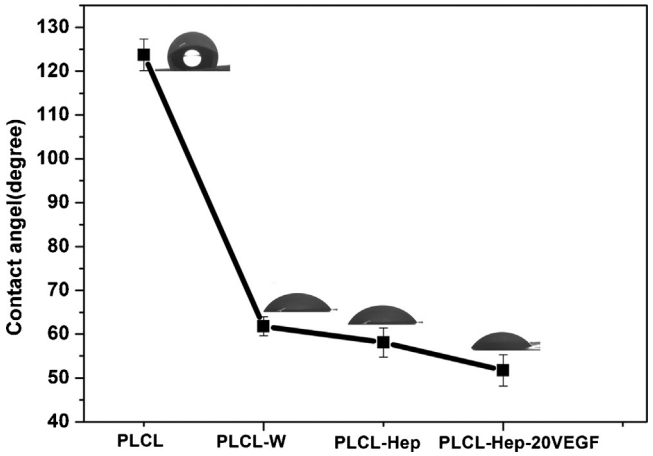

Fig. 3. Water contact angles of electrospun nanofiber mats ($n = 3$). The insets show images of the water droplets after they were placed on the nanofiber mats.

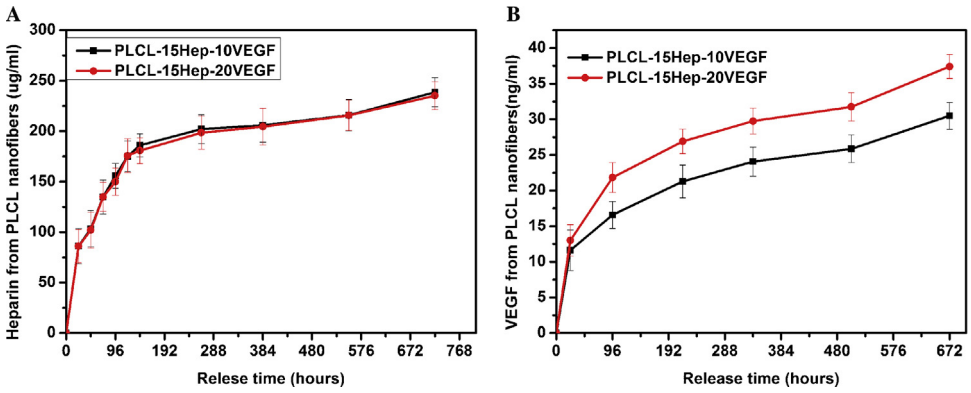

Fig. 4. Release profile of heparin (A) and VEGF (B) released from fiber mats ($n = 3$).

profiles of heparin and VEGF were mainly composed of two stages. As shown in Fig. 4A, a gradual sustained release of heparin occurred until day 6, followed by a slow release until day 29. There was no significant difference in the release profiles of heparin released from PLCL-15Hep-10VEGF and that released from PLCL-15Hep-20VEGF. This suggests that the presence of VEGF in small amounts has no effect on the release behavior of heparin. During the 29 day study, the quantity of Vheparin per milliliter of medium reached approximately 240 μg. As shown in Fig. 4B, the release profiles of VEGF and heparin are slightly different. The amount of heparin is greater than that of VEGF; as a result, the existence of heparin affected the release of VEGF. VEGF was released at a high rate from both the PLCL-15Hep-10VEGF and PLCL-15Hep-20VEGF fiber mats for the first 4 days, followed by a gradual sustained release. More VEGF was released from PLCL-15Hep-20VEGF than from PLCL-15Hep-10VEGF due to the higher loading amount of VEGF. After 28 days, approximately 30 and 37 ng of VEGF per milliliter of release medium were released from the PLCL-15Hep-10VEGF and PLCL-15Hep-20VEGF fiber mats, respectively. All of these results indicated that the heparin and VEGF loaded in the fiber mats could be released in a controlled manner. The amount of VEGF released is affected by the loading quantity and the co-encapsulation of heparin.

3.4. Hemocompatibility assessment

3.4.1. Hemolysis test

The fundamental requirement for biomaterials is biocompatibility. For potential intravascular graft materials, the first step is to evaluate blood compatibility. As a xenogenous graft, the physical and chemical agents on its surface could damage erythrocytes, leading to the release of hemoglobin. The hemolysis test is based on the degree of erythrolysis that occurs when the material contacts erythrocytes in vitro and is widely used to evaluate the destructive potential that implants present to erythrocytes. The lower the hemolysis rate, the better the hemocompatibility. According to previous studies, 5% is the criterion for excellent blood compatibility [25].

Fig. 5 shows that all of the rates were <5%, indicating that all of the nanofibers had good blood compatibility. The rates of PLCL-10Hep and PLCL-15Hep fibers were less than 0, meaning they had even fewer ruptured erythrocytes than the negative control. This could be because, in addition to its well-known anticoagulant properties, heparin also acts as a complement activation regulator [26]. Mannari et al. [27] suggest that heparin plays an important role in the management of complement-mediated hemolytic processes.

3.4.2. Platelet adhesion test

In addition to a low erythrolytic rate, good blood compatibility also requires that a material does not induce coagulation. The inhibition of thrombogenesis is a priority for materials in contact with blood. The platelet adhesion test is a common evaluation of the thrombogenicity of blood-contacting materials [28]. Fig. 6 demonstrates that the number of platelets adhering to the surfaces of PLCL-5Hep, PLCL-10Hep and PLCL-15Hep nanofiber mats was lower than the number of cells adhered to pure PLCL nanofiber mats, and this disparity increased as the concentration of heparin increased. It revealed a dose-dependent anti-coagulating effect for the heparin-loading nanofibers.

3.5. Biocompatibility assessment

3.5.1. Identification of rat bone marrow derived EPCs

After being cultured for 7 days in vitro, the expanded mononuclear cells derived from the bone marrow of SD rats had attached to culture dishes and formed multiple cell clusters (Fig. 7a). After two passages, the P2 cells were used for immunofluorescent staining and FACS analysis. After being incubated with Ac-LDL (10 mg/mL) for 4 h at 37 °C, EPCs were counterstained with FITC-conjugated UEA-1-lectin. As shown in Fig. 7a, the majority of these cells took up both molecules. Further analysis by FACS demonstrated that (Fig. 7b) double-positive cells (CD34 and KDR) accounted for more than 80% of all cells.

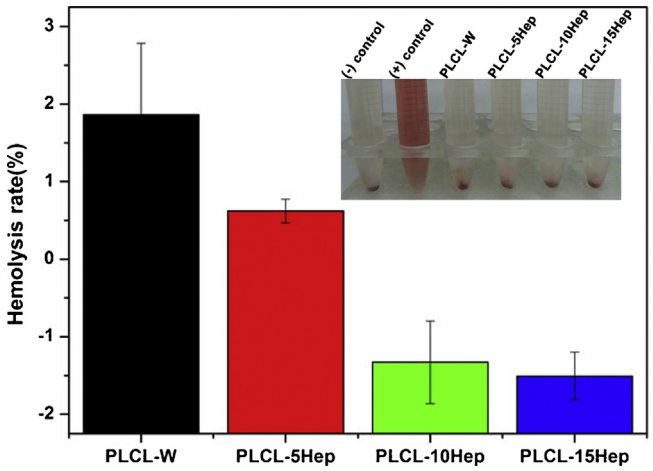

Fig. 5. Hemolysis rates of the four types of nanofibers in contact with blood in vitro ($n = 3$). The inset photograph shows the hemolytic condition after centrifugation. All four sample types had acceptable hemolysis rates (<5%).

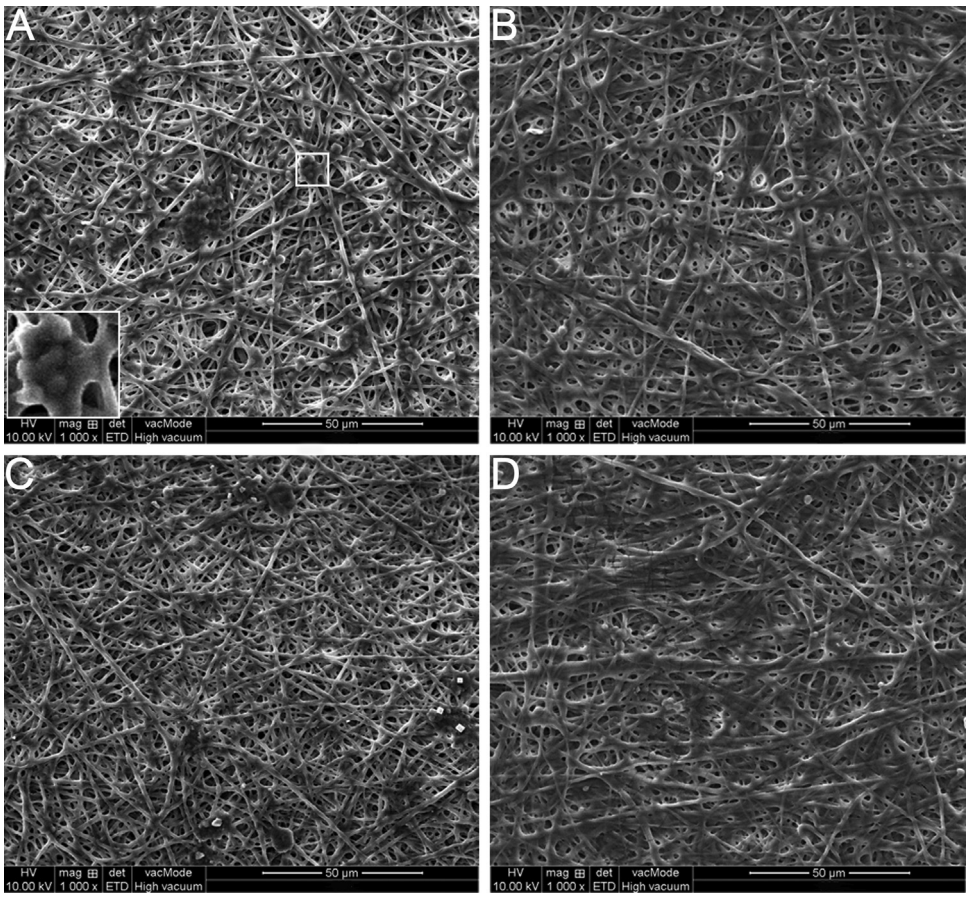

Fig. 6. SEM images of the platelets adhesion on (A) PLCL, (B) PLCL-5Hep, (C) PLCL-10Hep, and (D) PLCL-15Hep nanofiber mats.

3.5.2. Cell proliferation and morphology assay

Fig. 8b shows that the absorbance of VEGF-containing nanofibers was significantly higher than those without VEGF ($p < 0.05$), especially at day 7. This finding indicates that EPCs proliferate faster on VEGF-loaded nanofibers than on those without VEGF and that the promoting effect was dose- and time-dependent. However, there was no significant difference between PLCL-15Hep-20VEGF and PLCL-15Hep-30VEGF, although the latter's numbers were slightly higher. Immunofluorescent staining (Fig. 8c) revealed the morphology and quantity of EPCs. Cell morphology and the

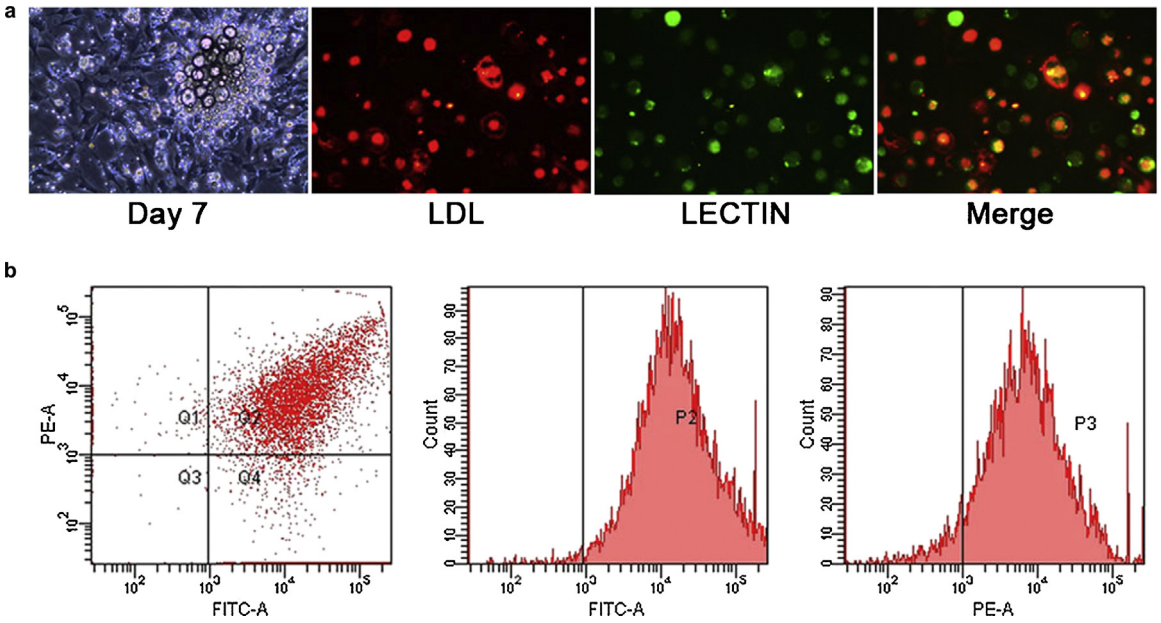

Fig. 7. (a) Mononuclear cells from bone marrow formed clusters on the 7th day of cultivation in vitro. Immunofluorescent staining showed that most of the cells could be double-stained and (b) fluorescence-activated cell sorting detected that double-positive cells (CD34 and KDR) accounted for more than 80%.

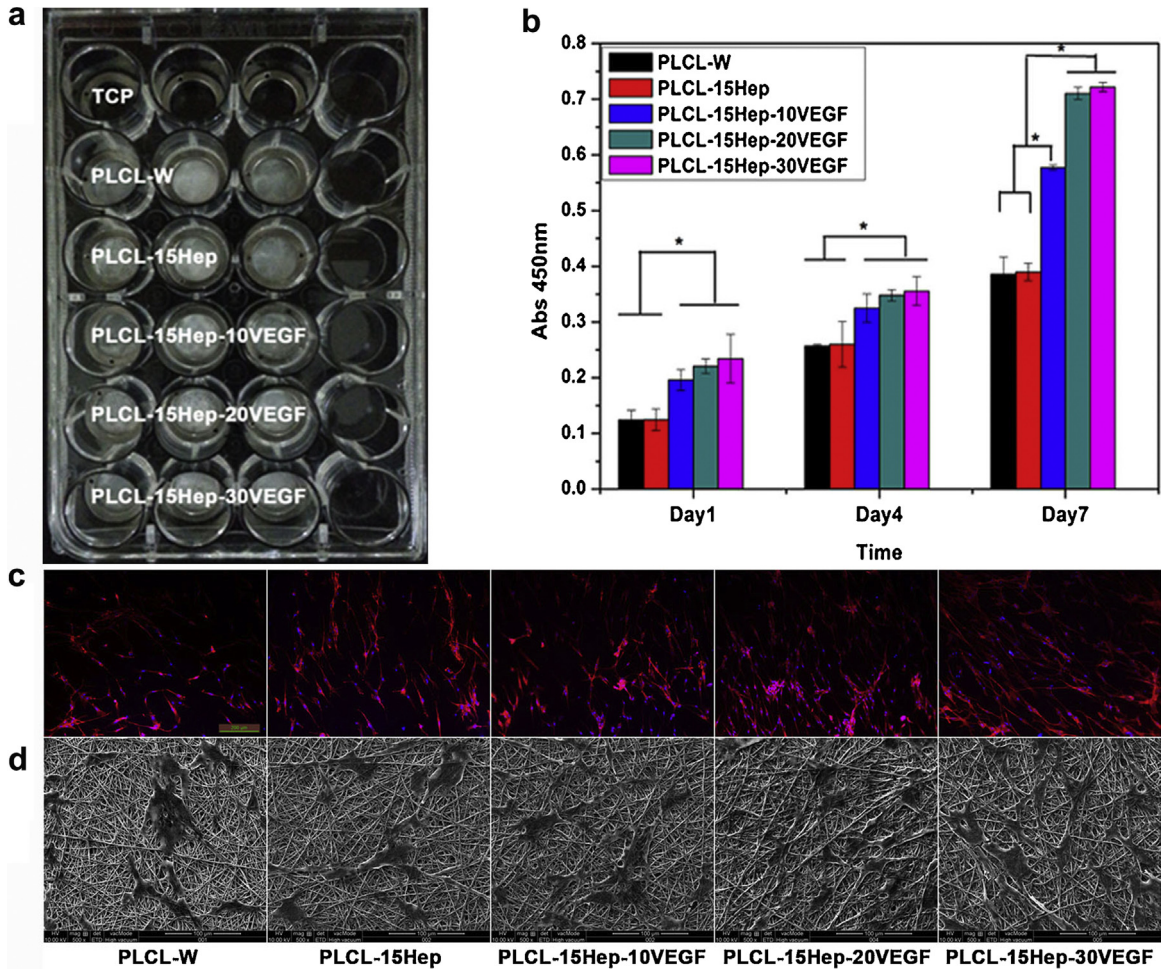

Fig. 8. (a) Illustration of the distribution of 5 types of nanofibers placed in a 24-well plate. The TCP group was used for observation during cultivation because the fibers were lightproof. (b) The proliferation of EPCs on 5 types of nanofiber mats was studied by CCK-8 assay ($n = 3$). The * symbol marks a significant difference between two groups. (c) and (d) Immunofluorenscent and SEM images of EPCs grown on the nanofiber mats.

interaction between EPCs and nanofibers were investigated using SEM. It can be observed in Fig. 8d that after 7 days of cultivation, EPCs spread well on the surface of the VEGF-loaded nanofibers and integrated well with the surrounding fibers.

Intravascular grafts are conduits placed in the targeted vessels to manage vascular diseases. Generally, there are two types of grafts: natural tissue or decellularized-matrix and synthetic materials. The former includes veins [29], arteries [30,31] and other forms of natural tissues (for example, pericardium [32]). Because of the absence of immunorejection, autografts are the preferred option. However, an inadequate supply of autologous vessels in some patients limits their use [33]. Furthermore, the performance of autografts is not always satisfactory in high-pressure arterial sites due to mechanical mismatch, which leads to the formation of aneurysms, intimal hyperplasia, and accelerated atherosclerosis [34,35]. Under such circumstances, synthetic alternatives that are not only compatible with the high-pressure environment but also have properties similar to those of the native tissues are needed. Because of their availability and controllable properties, synthetic grafts have been widely used in the treatment of various diseases, such as coronary or peripheral artery bypasses for revascularization [36], arteriovenous fistulae for dialysis [37] and covered stents for aneurysm occlusion [38,39]. It has been observed, however, that thrombogenesis and intimal hyperplasia occur relatively frequently when prosthetic grafts are used [40,41]. As is well known, the endothelium, the primary border between the circulating blood and the vascular wall, secretes a variety of anti-coagulant and anti-inflammatory factors [42], thus acting as a non-adhesive surface for platelets and leukocytes. Therefore, it is speculated that the early presence of a functional endothelial monolayer after intravascular graft implantation could reduce the risk of thrombogenesis and restenosis. In fact, active re-endothelialization could prevent inflammatory activation, thereby avoiding further platelet adhesion and restenosis [43]. In the past, regeneration of the endothelium was solely attributed to the migration and proliferation of adjacent endothelial cells. This dogma was overturned in 1997 after Asahara et al. found that $CD34^+$ mononuclear cells isolated from peripheral blood could differentiate into endothelial phenotypes in vitro [9]. These cells, named endothelial progenitor cells (EPCs), express various endothelial markers [9,44], including KDR (VEGF receptor-2), CD34, and VE-cadherin, so additional repair mechanisms may exist. Bone marrow transplantation experiments revealed that bone marrow-derived EPCs contributed to endothelialization on the surface of grafts and denuded arteries [45,46]. The recruitment of EPCs to the site of a vascular injury was shown to inhibit neointimal hyperplasia and restenosis [47]. Therefore, it is now widely recognized that circulating EPCs aid in the regeneration of damaged and dysfunctional endothelium and therefore play a central role in the vascular repair process [10]. The mobilization, recruitment, proliferation and homing of EPCs is not yet fully understood, but it has been demonstrated that EPCs are modulated by a variety of cytokines (e.g., granulocyte colony stimulating

factor [48] and erythropoietin [49]), growth factors (e.g., vascular endothelial growth factor [7,50]) and drugs (e.g., statins [51,52]) and are influenced by many conditions, such as ischemia [53] or vessel wall damage [54]. Of all the factors listed above, VEGF is possibly the most thoroughly studied. It has been doubly proven that VEGF contributes to the mobilization of EPCs; VEGF gene transfer augmented the population of EPCs, and blocking the VEGFR 2 signaling pathway had a negative effect on the EPCs [55]. Therefore, in our study, we encapsulated VEGF into electrospun nanofibers and evaluated its ability to promote EPC viability by means of a CCK assay. We found that VEGF had a dose- and time-responsive stimulated impact. Immunofluorescent staining and SEM micrographs of cells grown under the same conditions also revealed a more stretched morphology and improved interaction with the surrounding fibers, possibly implying firmer immobilization of EPCs due to the chemotaxis induced by VEGF.

4. Conclusion

In summary, we successfully encapsulated heparin and VEGF into nanofibers via emulsion electrospinning. The morphology and interior structure of the fibers was observed by SEM and TEM. The surface hydrophilicity was evaluated by measuring the water contact angle. The results indicated that nanofibers containing heparin/VEGF (PLCL-Hep, and PLCL-Hep-20VEGF) were smaller in diameter than pure PLCL nanofibers. The hydrophilicity test suggested that the addition of emulsifier and heparin/VEGF improved the surface hydrophilicity of nanofiber mats. It was demonstrated by hemolysis and platelet adhesion testing that the nanofiber mats fabricated via emulsion electrospinning have excellent blood compatibility. With regard to their effects on EPCs, the CCK-8 assay also showed that the VEGF-containing nanofibers promoted EPC growth in a dose- and time-dependent manner. Therefore, this new type of nanofiber can be generalized to various vascular grafts whose application is limited by thrombogenesis and restenosis.

Acknowledgments

This research was financially supported by the National Natural Science Foundation of China (nos. 30973105 and 31271035) and the Shanghai City Committee of Science and Technology of Nano Special (11nm 0504100 and 11nm 0506200).

References

[1] P. Zilla, D. Bezuidenhout, P. Human, Biomaterials 28 (2007) 5009.
[2] M. Desai, A.M. Seifalian, G. Hamilton, Eur. J. Cardiothorac. Surg. 40 (2011) 394.
[3] J. Hirsh, S.S. Anand, J.L. Halperin, V. Fuster, American Heart Association, Arterioscler. Thromb. Vasc. Biol. 21 (2001) E9.
[4] R.A. Hoshi, R. Van Lith, M.C. Jen, J.B. Allen, K.A. Lapidos, G. Ameer, Biomaterials 34 (2013) 30.
[5] F.P. Seib, M. Herklotz, K.A. Burke, M.F. Maitz, C. Werner, D.L. Kaplan, Biomaterials 35 (2014) 83.
[6] Y. Yao, J. Wang, Y. Cui, R. Xu, Z. Wang, J. Zhang, K. Wang, Y. Li, Q. Zhao, D. Kong, Acta Biomater. 10 (2014) 2739.
[7] T. Asahara, T. Takahashi, H. Masuda, C. Kalka, D. Chen, H. Iwaguro, Y. Inai, M. Silver, J.M. Isner, EMBO J. 18 (1999) 3964.
[8] L. Coultas, K. Chawengsaksophak, J. Rossant, Nature 438 (2005) 937.
[9] T. Asahara, T. Murohara, A. Sullivan, M. Silver, R. van der Zee, T. Li, B. Witzenbichler, G. Schatteman, J.M. Isner, Science 275 (1997) 964.
[10] M. Hristov, W. Erl, P.C. Weber, Arterioscler. Thromb. Vasc. Biol. 23 (2003) 1185.
[11] S. Takeshita, L.P. Zheng, E. Brogi, M. Kearney, L.Q. Pu, S. Bunting, N. Ferrara, J.F. Symes, J.M. Isner, J. Clin. Invest. 93 (1994) 662.
[12] Q.P. Pham, U. Sharma, A.G. Mikos, Tissue Eng. 12 (2006) 1197.
[13] H. Jiang, Y. Hu, Y. Li, P. Zhao, K. Zhu, W. Chen, J. Control. Release 108 (2005) 237.
[14] X. Xu, L. Yang, X. Xu, X. Wang, X. Chen, Q. Liang, J. Zeng, X. Jing, J. Control. Release 108 (2005) 33.
[15] H. Zhang, C.G. Zhao, Y.H. Zhao, G.W. Tang, X.Y. Yuan, Sci. China Chem. 53 (2010) 1246.
[16] X. Li, Y. Su, S. Liu, L. Tan, X. Mo, S. Ramakrishna, Colloids Surf. B: Biointerfaces 75 (2010) 418.
[17] S.Y. Chew, J. Wen, E.K. Yim, K.W. Leong, Biomacromolecules 6 (2005) 2017.
[18] M.P. Prabhakaran, J.R. Venugopal, S. Ramakrishna, Biomaterials 30 (2009) 4996.
[19] X.M. Mo, C.Y. Xu, M. Kotaki, S. Ramakrishna, Biomaterials 25 (2004) 1883.
[20] M. Tanaka, T. Motomura, M. Kawada, T. Anzai, Y. Kasori, T. Shiroya, K. Shimura, M. Onishi, A. Mochizuki, Biomaterials 21 (2000) 1471.
[21] S. Yan, L. Xiaoqiang, L. Shuiping, M. Xiumei, S. Ramakrishna, Colloids Surf. B: Biointerfaces 73 (2009) 376.
[22] Y. Liao, L. Zhang, Y. Gao, Z.T. Zhu, H. Fong, Polymer 49 (2008) 5294.
[23] L. Wu, H. Li, S. Li, X. Li, X. Yuan, X. Li, Y. Zhang, J. Biomed. Mater. Res. A 92 (2010) 563.
[24] H.Y. Wang, Y.K. Feng, W.J. Yuan, H.Y. Zhao, Z.C. Fang, M. Khan, J.T. Guo, Sci. China Phys. Mech. 55 (2012) 1189.
[25] M.A. Dobrovolskaia, J.D. Clogston, B.W. Neun, J.B. Hall, A.K. Patri, S.E. McNeil, Nano Lett. 8 (2008) 2180.
[26] H. Ninomiya, Y. Kawashima, T. Nagasawa, Br. J. Haematol. 109 (2000) 875.
[27] D. Mannari, C. Liu, D. Hughes, A. Mehta, Acta Haematol. 119 (2008) 166.
[28] D.K. Han, S.Y. Jeong, Y.H. Kim, J. Biomed. Mater. Res. 23 (Suppl.) (1989) 211.
[29] J.F. Sabik 3rd, Circulation 124 (2011) 273.
[30] S. Verma, P.E. Szmitko, R.D. Weisel, D. Bonneau, D. Latter, L. Errett, Y. LeClerc, S.E. Fremes, Circulation 110 (2004) e40.
[31] C.X. Gu, J.F. Yang, H.C. Zhang, H. Wei, L.K. Li, J. Geriatr. Cardiol. 9 (2012) 247.
[32] I. Vulev, A. Klepanec, R. Bazik, T. Balazs, R. Illes, J. Steno, Interv. Neuroradiol. 18 (2012) 164.
[33] R.Y. Kannan, H.J. Salacinski, P.E. Butler, G. Hamilton, A.M. Seifalian, J. Biomed. Mater. Res. B: Appl. Biomater. 74 (2005) 570.
[34] J.D. Lee, M. Srivastava, J. Bonatti, Circ. J. 76 (2012) 2058.
[35] C.D. Owens, N. Wake, M.S. Conte, M. Gerhard-Herman, J.A. Beckman, J. Vasc. Surg. 50 (2009) 1063.
[36] A. Tiwari, H. Salacinski, A.M. Seifalian, G. Hamilton, Cardiovasc. Surg. 10 (2002) 191.
[37] P. Dutka, H. Brickel, Nephrol. Nurs. J. 37 (2010) 531, quiz, 536.
[38] U. Blum, G. Voshage, J. Lammer, F. Beyersdorf, D. Töllner, G. Kretschmer, G. Spillner, P. Polterauer, G. Nagel, T. Hölzenbein, N. Engl. J. Med. 336 (1997) 13.
[39] I. Saatci, H.S. Cekirge, M.H. Ozturk, A. Arat, F. Ergungor, Z. Sekerci, E. Senveli, U. Er, S. Turkoglu, O.E. Ozcan, T. Ozgen, AJNR Am. J. Neuroradiol. 25 (2004) 1742.
[40] P. Roy-Chaudhury, B.S. Kelly, M.A. Miller, A. Reaves, J. Armstrong, N. Nanayakkara, S.C. Heffelfinger, Kidney Int. 59 (2001) 2325.
[41] S. Nishi, Y. Nakayama, H. Ishibashi-Ueda, Y. Okamoto, Y. Kinoshita, J. Artif. Organs 12 (2009) 35.
[42] D.B. Cines, E.S. Pollak, C.A. Buck, J. Loscalzo, G.A. Zimmerman, R.P. McEver, J.S. Pober, T.M. Wick, B.A. Konkle, B.S. Schwartz, E.S. Barnathan, K.R. McCrae, B.A. Hug, A.M. Schmidt, D.M. Stern, Blood 91 (1998) 3527.
[43] J.F. Granada, S. Inami, M.S. Aboodi, A. Tellez, K. Milewski, D. Wallace-Bradley, S. Parker, S. Rowland, G. Nakazawa, M. Vorpahl, F.D. Kolodgie, G.L. Kaluza, M.B. Leon, R. Virmani, Circ. Cardiovasc. Interv. 3 (2010) 257.
[44] Q. Shi, S. Rafii, M.H. Wu, E.S. Wijelath, C. Yu, A. Ishida, Y. Fujita, S. Kothari, R. Mohle, L.R. Sauvage, M.A. Moore, R.F. Storb, W.P. Hammond, Blood 92 (1998) 362.
[45] S. Kaushal, G.E. Amiel, K.J. Guleserian, O.M. Shapira, T. Perry, F.W. Sutherland, E. Rabkin, A.M. Moran, F.J. Schoen, A. Atala, S. Soker, J. Bischoff, J.E. Mayer, Nat. Med. 7 (2001) 1035.
[46] N. Werner, S. Junk, U. Laufs, A. Link, K. Walenta, M. Bohm, G. Nickenig, Circ. Res. 93 (2003) e17.
[47] N. Kipshidze, G. Dangas, M. Tsapenko, J. Moses, M.B. Leon, M. Kutryk, P. Serruys, J. Am. Coll. Cardiol. 44 (2004) 733.
[48] M. Delgaudine, B. Lambermont, P. Lancellotti, V. Roelants, S. Walrand, J.L. Vanoverschelde, L. Pierard, A. Gothot, Y. Beguin, Cytotherapy 13 (2011) 237.
[49] C. Heeschen, A. Aicher, R. Lehmann, S. Fichtlscherer, M. Vasa, C. Urbich, C. Mildner-Rihm, H. Martin, A.M. Zeiher, S. Dimmeler, Blood 102 (2003) 1340.
[50] C. Kalka, H. Tehrani, B. Laudenberg, P.R. Vale, J.M. Isner, T. Asahara, J.F. Symes, Ann. Thorac. Surg. 70 (2000) 829.
[51] W. Wang, J.K. Lang, G. Suzuki, J.M. Canty Jr., T. Cimato, PLoS ONE 6 (2011) e24868.
[52] Y. Liu, J. Wei, S. Hu, L. Hu, Am. J. Med. Sci. 344 (2012) 220.
[53] S. Shintani, T. Murohara, H. Ikeda, T. Ueno, T. Honma, A. Katoh, K. Sasaki, T. Shimada, Y. Oike, T. Imaizumi, Circulation 103 (2001) 2776.
[54] M. Gill, S. Dias, K. Hattori, M.L. Rivera, D. Hicklin, L. Witte, L. Girardi, R. Yurt, H. Himel, S. Rafii, Circ. Res. 88 (2001) 167.
[55] C. Kalka, H. Masuda, T. Takahashi, R. Gordon, O. Tepper, E. Gravereaux, A. Pieczek, H. Iwaguro, S.I. Hayashi, J.M. Isner, T. Asahara, Circ. Res. 86 (2000) 1198.